On gravity currents propagating at the base of a stratified ambient

By MARIUS UNGARISH[1] AND HERBERT E. HUPPERT[2]

[1]Department of Computer Science, Technion, Haifa 32000, Israel

[2]Institute of Theoretical Geophysics,
Department of Applied Mathematics and Theoretical Physics, University of Cambridge,
Silver Street, Cambridge CB3 9EW, UK

The behaviour of an inviscid gravity current which is released from behind a lock and then propagates over a horizontal boundary at the base of a stratified ambient fluid is considered. An extension of the shallow-water formulation for a homogeneous ambient to the stratified case is developed, without using any additional adjustable parameters. Attention is focused on the initial 'slumping' stage of a rectangular current which is typified by a constant speed of propagation. The analytical results are in good agreement with, and give a firm theoretical interpretation of, the corresponding experiments and numerical simulations of Maxworthy *et al.* (2002). Finite-difference solutions of the Navier–Stokes equations, using a different technique from that used by Maxworthy *et al.* (2002), are also presented and provide both good agreement with their results and further validation of the present shallow-water approach. The differences between currents in a homogeneous and stratified ambient, and possible implementation of the results to other configurations, are discussed.

1. Introduction

Gravity currents occur whenever fluid of one density flows primarily horizontally into fluid of a different density. Many such situations arise in both industrial and natural settings, as reviewed by Simpson (1997) and Huppert (2000). Commonly the current is driven by compositional or temperature differences, to lead to a homogeneous current, or by suspended particulate matter, to lead to a particle-driven current (Bonnecaze, Huppert & Lister 1993; Bonnecaze *et al.* 1995; Huppert 1998), and combinations of both particle and compositional or temperature differences can also occur (Hogg, Hallworth & Huppert 1999). Currents may propagate in either a rectangular, two-dimensional or cylindrical, axisymmetric configuration, or may be otherwise influenced by sidewall and/or topographic constraints. Some of these processes have now been fairly well investigated. A typical investigation considers the instantaneous release of a constant volume of heavy fluid from behind a lock into a large reservoir of a less dense homogeneous fluid above an impermeable horizontal boundary. Our aim here is primarily to evaluate the effects of a stratified ambient on the propagation of high Reynolds number currents resulting from the instantaneous release of a finite volume of fluid of constant density in a rectangular two-dimensional geometry. Applications of our work include areas such as oceanography, atmospheric winds and environmental control.

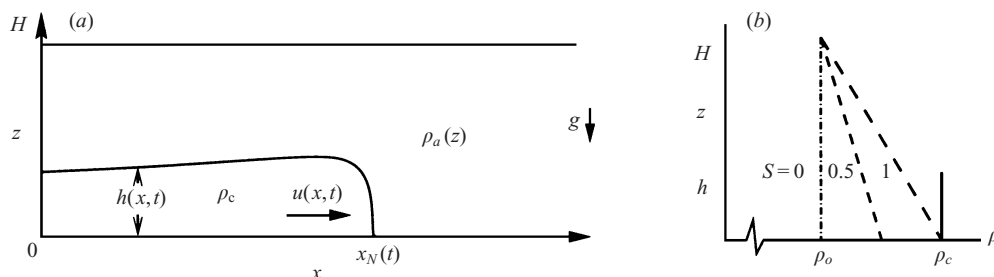A study of the prototype problem has been recently performed by Maxworthy

FIGURE 1. Schematic description of the system: (*a*) the geometry; and (*b*) the density profiles in the current (solid line) and ambient, for various values of S (dashed lines).

et al. (2002, referred to herein as MLSM). They considered the propagation of a saline current released from behind a lock over a horizontal bottom into a linearly stratified saline ambient in a rectangular container whose upper boundary was open to the atmosphere. The investigation was a combination of laboratory and numerical experiments. The numerical solutions, obtained from the full Boussinesq formulations, were in very good agreement with the measurements. Attention focused on the speed of propagation of the nose during the initial stage, for which a quite general data correlation was obtained, as we shall detail below.

This leaves open some important points, including: the interpretation of the reported experimental/numerical correlations in terms of fundamental concepts; the possibility of predicting the observed behaviour using a convenient shallow-water (SW) approximation (in extended formulation); and the behaviour in circumstances which were not covered by these experiments. The object of this paper is to study these matters.

The system under consideration is sketched in figure 1: a deep layer of ambient fluid, of density $\rho_a(z)$, lies above a horizontal surface at $z = 0$. Gravity acts in the negative z-direction. In the rectangular case the system is bounded by parallel vertical smooth impermeable surfaces and the current propagates in the direction labelled x. At time $t = 0$ a given volume of homogeneous fluid of density $\rho_c \geqslant \rho_a(z = 0) \equiv \rho_b$ and kinematic viscosity v, initially at rest in a rectangular box of height h_0 and length x_0, is instantaneously released into the ambient fluid. A two-dimensional current commences to spread. We assume that the Reynolds number of the horizontal flow, $Re_N = h_N u_N / v$, where the subscript N denotes values associated with the 'nose' of the current, is large and hence viscous effects can be neglected. In the experiments of MLSM, Re_N was estimated as typically 10^3 and hence the inviscid approach is appropriate. (After a significant spread and decay of both h_N and u_N viscous forces become important, but this phase is outside the scope of the present work.)

The corresponding flows with a homogeneous ambient, in particular in the rectangular configuration, have been extensively studied both experimentally and theoretically. Theoretical investigations successfully using the shallow-water approximation have been conducted. Further simplifications in the form of 'box models' have also been developed for obtaining quick estimates of the global behaviour. Numerical experiments based on simulations using the 'full' equations of motion (in the Boussinesq or Navier–Stokes formulations) have also been used recently for acquiring flow-field details which are not easily measured in laboratory experiments or incorporated into the simplified theory, see Klemp, Rotunno & Skamarock (1994), Härtel, Meiburg & Necker (2000) and Hallworth, Huppert & Ungarish (2001).

The structure of the paper is as follows. In §2 the model equations of motion, based on shallow-water approximations and the appropriate boundary conditions, are developed and some results are obtained. A comparison with the results of MLSM is performed in §3. Finite-difference solutions of the full Navier–Stokes equations and additional comparisons are discussed in §4. We present a summary of our results and some concluding remarks in §5.

2. Formulation and shallow-water approximation

The configuration is sketched in figure 1. For the rectangular case we use an $\{x, y, z\}$ Cartesian coordinate system with corresponding $\{u, v, w\}$ velocity components, and assume that the flow does not depend on the coordinate y and that $v \equiv 0$.

Initially, the height of the propagating current is h_0, its length is x_0 and the density is ρ_c. The height of the ambient fluid is H and the density in this domain decreases linearly with z from ρ_b to ρ_o. (The linear variation is taken here for simplicity of analysis, but is not essential; the subscripts b, o refer to bottom and open surface values respectively.)

It is convenient to use ρ_o as the reference density and to introduce the reduced density differences and ratios between them

$$\epsilon = \frac{\rho_c - \rho_o}{\rho_o}, \quad \epsilon_b = \frac{\rho_b - \rho_o}{\rho_o}, \tag{2.1}$$

and

$$S = \epsilon_b / \epsilon, \tag{2.2}$$

from which it follows that

$$\rho_c = \rho_o(1 + \epsilon), \quad \rho_a = \rho_o \left[1 + \epsilon S \left(1 - \frac{z}{H} \right) \right], \tag{2.3}$$

where S represents the magnitude of the stratification in the ambient fluid, and we shall consider only $0 \leqslant S \leqslant 1$. The homogeneous ambient is recovered by setting $S = 0$. (MSLM used the parameter R, the inverse of S, to express the stratification in the ambient fluid, but we find S to be more convenient.) We also define the reference reduced gravity,

$$g' = \epsilon g, \tag{2.4}$$

where g is the gravitational acceleration, and we keep in mind that the effective reduced gravity which actually drives the current is smaller than the quantity defined in (2.4) because of the stratification. It is convenient for purposes of interpretation to keep in mind the following picture, also sketched in figure 1(*b*): $S = 0$ corresponds to a homogeneous ambient of density ρ_o and a current of fluid of density ρ_c. For $0 < S < 1$ the density of the ambient is stratified (increases linearly) from the same ρ_o at the top to a larger density at the bottom. The extreme situation $S = 1$ is achieved when the density of the ambient at the base matches that of the current.

We shall use a one-layer approximation which is expected to capture many of the important features of the flow, although it filters out internal waves in the ambient, and is the simplest shallow-water model. In the ambient fluid domain we assume that $u = v = w = 0$ and hence the fluid is in purely hydrostatic balance and maintains the initial density $\rho_a(z)$. The motion is assumed to take place in the lower layer only, $0 \leqslant x \leqslant x_N(t)$ and $0 \leqslant z \leqslant h(x, t)$. As in the classical inviscid, shallow-water analysis of a gravity current in a homogeneous ambient, we argue that the predominant

vertical momentum balance in the current is hydrostatic and that viscous effects in the horizontal momentum balance are negligibly small. Hence the motion is governed by the balance between pressure and inertia forces in this horizontal direction. As in the situation with a homogeneous ambient, an order-of-magnitude analysis indicates that the perturbation of the upper free surface introduced by the flow can be neglected when $\epsilon \ll 1$, as assumed here.

A relationship between the pressure fields and the height $h(x,t)$ can be obtained. In the motionless ambient fluid, which is open to the atmosphere, the pressure does not depend on x, and the hydrostatic balances $\partial p_i/\partial z = -\rho_i g$, where $i = a$ or c, and use of (2.3) yield

$$p_a(z,t) = -\rho_o \left[1 + \epsilon S \left(1 - \frac{1}{2} \frac{z}{H} \right) \right] gz + C, \qquad (2.5)$$

$$p_c(x,z,t) = -\rho_o(1 + \epsilon)gz + f(x,t), \qquad (2.6)$$

where the constant C reflects the constant pressure at the top of the ambient at $z = H$. Pressure continuity between the ambient and the current on the interface $z = h(x,t)$ determines the function $f(x,t)$ of (2.6) and we obtain, after some algebra,

$$p_c(x,z,t) = -\rho_o(1 + \epsilon)gz + \rho_o g' \left[h - S \left(h - \frac{1}{2} \frac{h^2}{H} \right) \right] + C, \qquad (2.7)$$

and consequently

$$\frac{\partial p_c}{\partial x} = \rho_o g' \frac{\partial h}{\partial x} \left[1 - S \left(1 - \frac{h}{H} \right) \right]. \qquad (2.8)$$

The expressions for p_a, p_c and $\partial p_c/\partial x$ are given in some detail because they highlight the essential difference between the stratified and the homogeneous formulations. The contribution of the stratification to the horizontal pressure gradient, and to the whole set of SW equations of motion, is in the square-bracket term of (2.8), and the contribution of the stratification to the vertical pressure head which drives the 'nose' is in the square-bracket term of (2.7).

As expected, the effect of stratification on the gravity current, as reflected by the horizontal pressure gradient, increases as S increases. However, for a given value of S there is an additional contribution proportional to h/H which tends to diminish the influence of stratification. Indeed, for a density which increases from $z = H$ to $z = 0$, at a deeper level the current encounters a larger density (i.e. a smaller driving force) than at a higher level. Figure 2 illustrates the behaviour of the normalized reduced pressure, defined as $P_i = (p_i + \rho_o gz - C)/\rho_o g' h$ $(i = a, c)$, in the current and ambient for typical values of S with h/H as a parameter.

The fact that $\partial p_c/\partial x$ is not a function of z makes the subsequent derivation of the SW equations a straightforward extension of the homogeneous case. Indeed, the next step is to consider the z-average of the horizontal momentum equation, which, on account of (2.8) and in conjunction with volume continuity, produces a system of equations for $h(x,t)$ and for the averaged longitudinal velocity, $u(x,t)$.

2.1. *Governing SW equations*

It is convenient to scale the dimensional variables (denoted here by asterisks) by

$$\{x^*, z^*, h^*, H^*, t^*, u^*\} = \{x_0 x, h_0 z, h_0 h, h_0 H, T t, U u\}, \qquad (2.9)$$

where

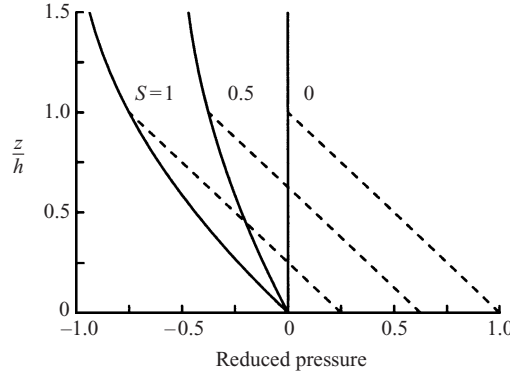$$U = (h_0 g')^{1/2} \quad \text{and} \quad T = x_0/U. \qquad (2.10)$$

FIGURE 2. The normalized reduced pressure as a function of the scaled height z/h: P_a (solid lines) and P_c (dashed lines) for $S = 0, 0.5$ and 1. (Here $h/H = 0.5$ and the curvature of P_a increases with h/H.)

Here h_0 and x_0 are the initial height and length of the current, U is a typical inertial velocity of propagation of the nose of the current and T is a typical time period for longitudinal propagation for a typical distance x_0. The scaling used here does not take into account the stratification; this will be reflected in the magnitude of the dimensionless results. Note that the horizontal and vertical lengths are scaled differently, which, as pointed out by Ungarish & Huppert (1999), removes the initial aspect ratio h_0/x_0 from the SW analysis in the homogeneous situation, and this applies also to the stratified case considered here.

The equations of motion can be conveniently expressed either for h and the combined variable (uh) in 'conservation form', or for the original variables in 'characteristic form', as follows.

2.2. *The governing equations*

In conservation form the equations can be written as

$$\frac{\partial h}{\partial t} + \frac{\partial}{\partial x}(uh) = 0, \qquad (2.11)$$

and

$$\frac{\partial}{\partial t}(uh) + \frac{\partial}{\partial x}\left[u^2 h + \tfrac{1}{2}(1-S)h^2 + \tfrac{1}{3}S\frac{h^3}{H}\right] = 0. \qquad (2.12)$$

In characteristic form these become

$$\begin{bmatrix} h_t \\ u_t \end{bmatrix} + \begin{bmatrix} u & h \\ 1-S+S(h/H) & u \end{bmatrix} \begin{bmatrix} h_x \\ u_x \end{bmatrix} = \begin{bmatrix} 0 \\ 0 \end{bmatrix}. \qquad (2.13)$$

For completeness, we also formulate the corresponding equations for the axisymmetric case. The current is released from a cylindrical lock of height h_0 and radius r_0, and the latter replaces x_0 in the scalings. Here we use a cylindrical coordinate system $\{r, \theta, z\}$ with corresponding $\{u, v, w\}$ velocity components, and assume that the flow does not depend on the angular coordinate θ and that $v \equiv 0$. In conservation form the equations can be written as

$$\frac{\partial h}{\partial t} + \frac{\partial}{\partial r}(uh) = -\frac{uh}{r}, \qquad (2.14)$$

and

$$\frac{\partial}{\partial t}(uh) + \frac{\partial}{\partial r}\left[u^2 h + \tfrac{1}{2}(1-S)h^2 + \tfrac{1}{3}S\frac{h^3}{H}\right] = -\frac{u^2 h}{r},\tag{2.15}$$

which in characteristic form become

$$\begin{bmatrix} h_t \\ u_t \end{bmatrix} + \begin{bmatrix} u & h \\ 1 - S + S(h/H) & u \end{bmatrix}\begin{bmatrix} h_r \\ u_r \end{bmatrix} = \begin{bmatrix} -uh/r \\ 0 \end{bmatrix}.\tag{2.16}$$

Note the existence of a non-zero right-hand-side in (2.16), in contrast to (2.13), which makes the development of the theory different for the axisymmetric situation. This will be detailed in a separate publication.

2.3. *Characteristics and boundary conditions*

The characteristic paths and relationships provide useful information for the solution of the system, including a proper definition of boundary conditions for the interface height h at the ends of the current domain. The stratification contributes to the pertinent results as follows.

Consider the equations of motion (2.13). Following the standard procedure for deriving the characteristic relationships, we calculate the eigenvalues of the matrix of coefficients of the space derivatives of the variables, which provide the speeds of propagation as

$$\lambda_{\pm} = u \pm \left[h\left(1 - S + S\frac{h}{H}\right)\right]^{1/2},\tag{2.17}$$

and the corresponding eigenvectors

$$(\pm a(h), 1),\tag{2.18}$$

where

$$a(h) = \left[\frac{1 - S + S(h/H)}{h}\right]^{1/2}.\tag{2.19}$$

Consequently, the relationships between the variables on the characteristics with $dx/dt = \lambda_{\pm}$, are

$$a(h)\,dh \pm du = 0.\tag{2.20}$$

The initial conditions are zero velocity and unit dimensionless height and length at $t = 0$. Also, the velocity at $x = 0$ is zero, and an additional condition is needed at the nose $x = x_N(t)$.

2.4. *The nose velocity*

The boundary condition for the velocity at the nose is essential for a proper physical definition and mathematical closure of the problem. The appropriate condition for the homogeneous ambient has been well studied, both theoretically and experimentally (Benjamin 1968; Huppert & Simpson 1980; Rottman & Simpson 1983). There is strong evidence that the velocity of the nose is proportional to the square-root of the pressure head (per unit mass), and that the factor of proportionality, defined as the Froude number Fr, varies in a quite narrow range with the ratio h_N/H. We argue that this result reflects a local, quasi-steady integral property of the current head and hence it is expected to remain valid also for a stratified ambient. We do not pursue a theoretical proof of this argument; rather, we use it as a base to develop measurable results (in particular, the velocity of the nose), and claim that agreement with experiments vindicates the assumption.

We define the effective pressure head as given by the difference between the pressure at the furthest point in the current and that in the ambient ahead of the current at the bottom ($z = 0$). Using the previously derived expressions for p_a and p_c when $h = h_N$, see also figure 2, we obtain the effective pressure head (scaled by $\rho_o g' h_0$) as

$$\left[h_N - S \left(h_N - \frac{1}{2} \frac{h_N^2}{H} \right) \right] \tag{2.21}$$

and consequently,

$$u_N = Fr \, h_N^{1/2} \times \left[1 - S \left(1 - \frac{1}{2} \frac{h_N}{H} \right) \right]^{1/2}. \tag{2.22}$$

The term in the square brackets of (2.22) is equal to 1 in the non-stratified case ($S = 0$), and smaller than 1 for $S > 0$. This term expresses the explicit slow-down of the head due to stratification effects. We notice that the expression in the square brackets is actually $[\rho_c - \rho_a(z = 0.5h_N)]/\epsilon \rho_o$. Thus, formally, the head reacts to the density difference at the middle of its height, which is larger than zero (and hence induces motion) even in the extreme case when $\rho_c = \rho_b$ (i.e., $S = 1$). Again, the stratification effect decreases as S decreases and when h_N/H increases (in both cases, the square-bracket term becomes closer to 1).

We now assume, and later vindicate by comparisons with numerous independent results, that the behaviour of Fr in the stratified case is approximated well by the well-known homogeneous situation, as follows. Benjamin (1968) proved that Fr is a decreasing function of h_N/H. Experiments confirmed this qualitative behaviour, but also indicated that the theoretical value of Fr, derived by Benjamin (1968) for a highly idealized motion, needs some modifications (a reduction of typically 20%) in real circumstances. To reconcile theory with practice, Huppert & Simpson (1980) developed the following simple well-known curve-fit type correlation which we shall also use here:

$$Fr = \begin{cases} 1.19 & (0 \leqslant h_N/H \leqslant 0.075) \\ 0.5 H^{1/3} h_N^{-1/3} & (0.075 \leqslant h_N/H \leqslant 1). \end{cases} \tag{2.23}$$

The scatter of the data used to obtain this formula suggests an estimate of $\pm 5\%$ for the error in this correlation, though later experiments and calculations by Rottman & Simpson (1983) suggest that, in some circumstances, the values for small h_N/H are about 15% smaller than predicted by (2.23). These discrepancies appear because in real gravity currents various departures from the idealized model are unavoidable, such as the complex three-dimensional structure of the head, time dependence, turbulent mixing, entrainment, friction, etc. Although each one of these effects is expected to be small, their accumulated contribution may be significant. It is therefore unlikely that a more accurate general one-parameter simple fit can be obtained. We therefore adopt (2.23) as a prototype correlation in the following work, but it will be evident that the essence of the analysis and conclusions are not affected by small details of the functional form of $Fr(h_N/H)$.

This closes the SW formulation. In general, the resulting system requires a numerical solution for the partial differential equations, but in the rectangular case some insightful results can be obtained by simpler, mostly analytical analysis, which we now proceed to develop.
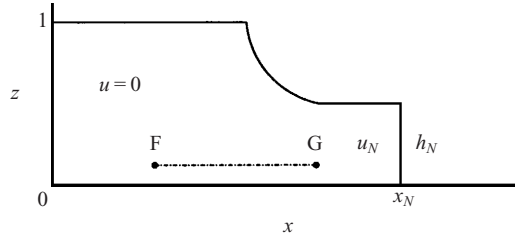
FIGURE 3. Schematic description of the current during the initial slumping stage.

2.5. *The slumping phase results*

A classical rectangular gravity current displays an initial 'slumping' stage of propagation with constant velocity and, accordingly, with constant h_N. Such a behaviour is also expected for the stratified current, as indicated by the fact that (2.20) admits a non-trivial solution with $dh = du = 0$. This has been confirmed by numerical computation performed in the framework of the present investigation. More importantly, MLSM observed this situation in all their experiments, and hence the results can serve for a stringent comparison.

The value of h_N during the slumping phase can be calculated as follows. In the current fluid domain sketched in figure 3, we follow a forward-propagating characteristic λ_+ from a point in the still unperturbed domain where $u = 0$ and $h = 1$ to a point in the domain where the velocity and the height have the constant values u_N and h_N. The connection between the variables at these points (F and G in the figure) is given from integrating (2.20) as

$$\int_{h_N}^{1} a(h)\,dh - u_N = 0. \tag{2.24}$$

The integral is a function of h_N, denoted $I(h_N)$, with S and H entering as parameters, and can be performed analytically, as presented in the Appendix §A.1. On the other hand, u_N is given by the Froude condition (2.22)–(2.23), and is also a function of h_N, with S and H entering as parameters. These substitutions transform (2.24) into

$$u_N = I(h_N) = Fr(h_N)\,h_N^{1/2}\left[1 - S\left(1 - \frac{1}{2}\frac{h_N}{H}\right)\right]^{1/2}, \tag{2.25}$$

a nonlinear equation for h_N, with S and H as parameters, whose numerical solution is straightforward. In the relevant domain $h_N \in (0, 1)$ the last term increases with h_N from zero, while $I(h_N)$ decreases with h_N to zero, and we found that there is a simple and unique root for a prescribed pair of S and H. For each $h_N(S, H)$ which satisfies (2.25), we can calculate the corresponding $u_N(S, H)$. This is the value of (2.25) when the equation is satisfied.

The results are presented in figure 4. As expected, the stratification hinders the propagation, i.e. u_N decreases when S increases for a fixed value of H. The reaction of the current to this hindrance is to pile up behind the front as reflected by the increase of h_N with S, but this is not a very pronounced feature. We note in passing that all the lines of u_N intersect at $S \approx 0.88$ which may indicate some eigenvalue of the system, but this issue has not been pursued.

The interesting case of $S = 1$ (i.e. $\rho_c = \rho_b$) and shallow current (when Fr is constant according to (2.23), $H > 7.4$), admits, somewhat surprisingly, an analytical result of (2.25). Using (A 7), substituting $S = 1$ and keeping in mind that Fr is now a constant,
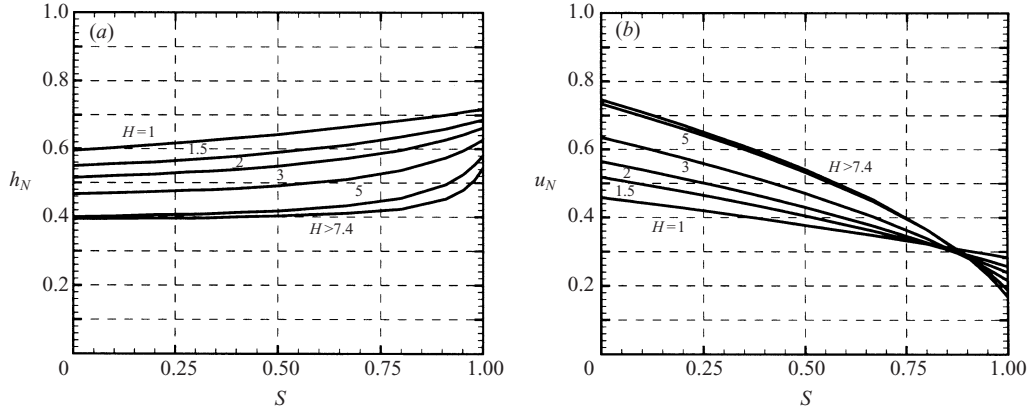
FIGURE 4. h_N and u_N as functions of S for various H.

(2.25) can be rewritten as

$$\frac{1}{H^{1/2}}(1 - h_N) = \sqrt{0.5}Fr\frac{1}{H^{1/2}}h_N. \tag{2.26}$$

For $Fr = 1.19$ this yields the results

$$h_N = 0.543, \quad u_N = \frac{0.457}{H^{1/2}}. \tag{2.27}$$

This velocity in dimensional form reads $0.457[(\rho_c - \rho_o)gh_0/\rho_o]^{1/2}(h_0/H)^{1/2}$, which can be explained in terms of our previous considerations as follows. Since at the bottom the current and the ambient have the same density, $\rho_a(z = 0) = \rho_b = \rho_c$, the current reacts to $\Delta\rho = \rho_a(z = 0.5h_N) - \rho_b = 0.5(\rho_c - \rho_o)h_N/H$. But $u_N \sim (\Delta\rho gh_N/\rho_o)^{1/2}$, in accordance with the original result.

Equation (2.22) indicates that for general S the dependence of u_N on the stratification is proportional to $[1 - S(1 - 0.5h_N/H)]^{1/2}$. However, h_N is not known *a priori*. Therefore, to estimate the behaviour of the current from the given initial conditions, it is necessary to use an approximation for h_N, and the foregoing results, see figure 4, indicate that $h_N \approx 0.5$. Figure 5 displays the velocity of the head re-scaled with the density difference at $z = 0.5h_N$ and also with this value approximated as 0.25. We observe that the results are lines almost parallel to the S-axis, which is a strong confirmation to our conjecture about the contribution of the stratification for a given H.

This suggests that the effective Froude number (based on the initially given value of h_0) can be conveniently defined, using dimensional variables, as

$$Fr_e = \frac{u_N}{(g'_e h_0)^{1/2}}, \tag{2.28}$$

where the 'effective' reduced gravity is given by

$$g'_e = \frac{\rho_c - \rho_a(z = 0.25h_0)}{\rho_o}g. \tag{2.29}$$

In the slumping stage the Froude number Fr_e varies over a rather small range: it increases from 0.5 to 0.9, approximately, as the thickness of the ambient H increases from 1 to ∞, and is roughly independent of the density factor S. This number seems
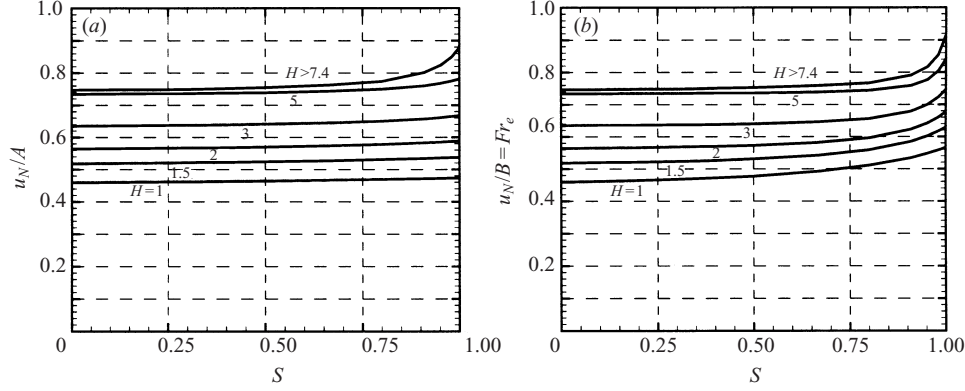
FIGURE 5. Rescaled u_N as a function of S for various H. (a) u_N/A with
$A = [1 - S(1 - 0.5h_N/H)]^{1/2}$; (b) $u_N/B = Fr_e$ with $B = [1 - S(1 - 0.25/H)]^{1/2}$.

to capture well the process under investigation. Furthermore, we show that a practical approximation for Fr_e is provided by the homogeneous Fr correlation (2.23).

To estimate the slumping distance, x_s, we observe that there are two phases during which the speed of propagation is constant. First, the entire current is flattened to a rectangular profile of height $z = h_N$ and, by continuity, of length $1/h_N$. Next, a depression wave propagates from the origin towards the nose, with velocity $u_N + \lambda_+$. The position of the nose when it is reached (and presumably affected) by this wave is

$$x_s = \frac{1}{h_N} \left(1 + \frac{u_N}{\lambda_+}\right). \tag{2.30}$$

Using the previous results for h_N, u_N and λ_+ we find that the stratification decreases the slumping distance. Equation (2.30) predicts that, for $S = 0$, $x_s = 2.3$ for $H = 1$ and increases to 3.9 when $H \geqslant 7.4$; and for $S = 1$ the corresponding values of x_s are 1.9 and 2.8. However, these results must be treated with care because there are experimental indications that the slumping distance of a current is a delicate feature involving quite complex wave interactions, and it seems that the SW approximation (and in particular the one-layer model result (2.30)) significantly underpredicts the slumping distance for the homogeneous ambient current (see Rottman & Simpson 1983, figure 11). In the stratified case internal waves in the ambient are also involved. In any case, the available experimental and numerical data suggest that (2.30) provides a lower bound for this property in both stratified and homogeneous situations. This whole aspect needs more investigation and is left for future work.

3. Comparison with and interpretation of MLSM's results

MLSM observed in all their experiments a significant stage of initial motion with constant velocity, and used the results to show that the (dimensional) velocity of the head scaled with $(\epsilon_b g H h_0)^{1/2}$ is independent of the initial aspect ratio h_0/x_0 and is a function of only S and H (recall, here H is the height of the ambient scaled with h_0) during this slumping stage. This observation is expressed in our notation as

$$\frac{u_N(\epsilon g h_0)^{1/2}}{(\epsilon_b g H h_0)^{1/2}} = \chi(S, H), \tag{3.1}$$
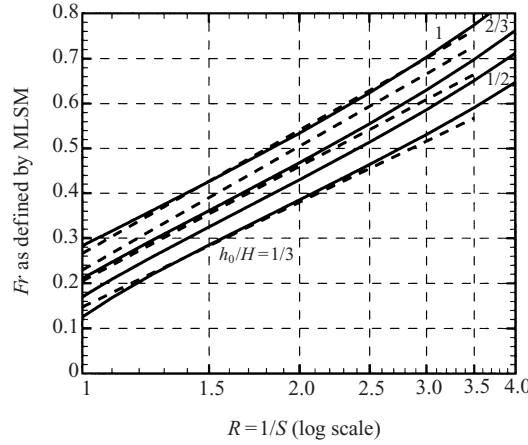
FIGURE 6. The behaviour of χ as a function of the stratification for various initial depth ratios, present results (solid lines) and the experimental fit of MLSM (dashed lines).

where u_N and H are dimensionless. MLSM determined an accurate experimental fit for $\chi(S, H)$ which is given in the Appendix § A.2. This is actually a Froude 'number', denoted Fr in MLSM, but we use a different notation to avoid confusion with our Fr.

We now show that the present SW theory results provide a theoretical interpretation of the experimentally obtained correlation (3.1). The considerations developed in the previous section indicate the existence of this constant-velocity slumping phase, and prove, using (2.22) and the present results for $h_N(S, H)$, that the left-hand-side of (3.1) is given by

$$\frac{1}{S^{1/2}} \left(\frac{h_N}{H}\right)^{1/2} Fr(h_N) \left[1 - S\left(1 - \frac{1}{2}\frac{h_N}{H}\right)\right]^{1/2},\tag{3.2}$$

which is a function of S and H only and can be identified as the theoretical form of $\chi(S, H)$. This expression is independent of h_0/x_0 since, as previously mentioned in § 2.1, this parameter has been scaled out from the present SW dimensionless formulation.

The first conclusion is that there is a perfect functional agreement between the present SW results and the experimental data of MLSM. Moreover, a quantitative comparison can be easily performed, and the results are presented in figure 6. The display uses the same axes and parametric values as figure 7 of MLSM. The laboratory and numerical experiments of MLSM were performed for $0.3 \leqslant S \leqslant 1$ and $H = 1, 1.5, 2$ and 3, and hence a comparison is relevant only for this range. We recall that the fitted curves are an accurate summary of the experimental data (with one exception detailed below) and hence the comparison in figure 6 is essentially between our theory and the data of MLSM.

The conclusion is that, for the relevant parameter range, the qualitative agreement is excellent, and the quantitative agreement can be considered very good. In detail, the closest agreements are for $h_0/H = 1/3$ and 1, with less good agreement for $h_0/H = 1/2$ and 2/3; the reason for this behaviour is at present not clear. The largest discrepancies are for values of S close to 1, but a detailed inspection of the experimental data reveals some scatter for this value of S, and actually the discrepancy here is at most 10%. Otherwise, the discrepancy between our theory and the experimental data is typically 5%; the worst agreement is for $H = 2$ (about 8%);

on the other hand, for $H = 1$ the discrepancy is almost zero. The agreement improves as S decreases, which reconfirms the semi-empirical evaluation of (2.23) on the basis of data taken from homogeneous currents. The discrepancies can be attributed to the various simplifications introduced in the SW formulation, and in particular the use of the one-layer model for non-large values of H and the neglect of internal waves in the ambient, and of mixing. Overall, we think that this is about the best agreement that can be expected from this type of modelling.

We emphasize that the present results were obtained by straightforward calculations without use of any additional adjustable parameters. (We employed the semi-empirical correlation (2.23) but this is a well-known ingredient of the SW approximations.) Consequently, we claim that the agreement with the experimental results of MLSM serves both as an interpretation of the observations and as a confirmation of our formulation.

It is remarkable that, as pointed out by MLSM, (3.2) (for a fixed H) is an almost perfect linear function of $\log S$ for $0.3 \leqslant S \leqslant 1$, but we could not find any theoretical argument to suggest this exact functional form. We speculate that this represents merely a good approximation, whose validity outside the range covered by the experiments of MLSM is questionable. For small values of S this functional approximation is bound to fail because (3.2) indicates that $\chi \sim S^{-1/2}$, not $\sim \log S$, for $S \rightarrow 0$. Indeed, for $S = 0.10$ the logarithmic fits of MLSM deviate by more than 15% from the present results, and for $S < 0.05$ the deviation is larger than 30%.

MLSM define the function χ as the Froude number of the current, and we introduced the definition (2.28) for the effective Froude number. The former definition has the advantage of linear dependence on $\log S$, but the disadvantage that it varies strongly with S in the range of interest and becomes invalid in the limit of the homogeneous ambient, $S = 0$. The latter definition has the advantage of small variation with S over the entire range, including the extreme cases $S = 1$ and 0.

4. Numerical results

We use a numerical finite-difference code which is a modified version of the software developed for the solution of an axisymmetric gravity current presented by Hallworth *et al.* (2001). The objectives are (*a*) to test the ability of the numerical solver to provide results for the stratified ambient, and (*b*) to obtain additional data for the verification of the present SW theory outside the domain covered by the data of MLSM.

For numerical convenience we introduce the density function $\phi(\boldsymbol{r}, t)$ by

$$\rho(\boldsymbol{x}, t) = \rho_o[1 + \epsilon\phi(\boldsymbol{x}, t)], \qquad (4.1)$$

where ϵ is the reduced density difference defined by (2.1). We expect $0 \leqslant \phi \leqslant 1$, with $\phi = 1$ in the domain of the 'pure' dense fluid and $0 \leqslant \phi \leqslant S$ in the domain of the ambient fluid.

We employ the following dimensionless balance equations:

conservation of volume

$$\nabla \cdot \boldsymbol{v} = 0; \qquad (4.2)$$

momentum balance

$$\frac{D\boldsymbol{v}}{Dt} = \frac{1}{1 + \epsilon\phi}\left[-\nabla P - \phi\hat{\boldsymbol{z}} + \frac{1}{Re}\nabla^2\boldsymbol{v}\right], \qquad (4.3)$$

where P is the reduced pressure (defined in dimensional form by $P = p + \rho_o g z$);

density transport

$$\frac{\partial \phi}{\partial t} + \nabla \cdot (\boldsymbol{v}\phi) = \mathscr{D}\nabla^2 \phi. \tag{4.4}$$

The relevant dimensionless parameters, in addition to ϵ, are the Reynolds number,

$$Re = \mathscr{U}\mathscr{L}/\nu, \tag{4.5}$$

and the dimensionless diffusion coefficient $\mathscr{D} = 1/Pe = 1/(\sigma Re)$, where Pe and σ are the Péclet and Schmidt numbers, respectively. Here $\mathscr{L}$ and $\mathscr{U}$ are the scaling length and velocity. In the numerical computations we employ $\mathscr{L} = x_0$ (the dimensional length of the lock) and $\mathscr{U} = (g'x_0)^{1/2}$. The scale for time is $\mathscr{L}/\mathscr{U}$.

We are interested in flows with large values of Re, small ϵ and very small $\mathscr{D}$. Actually, the typical physical value of $\mathscr{D}$ is negligibly small (recall that $\sigma \gg 1$ for saline solutions in water), but here a non-vanishing $\mathscr{D}$ is used in the solution of (4.4) as an artificial diffusion coefficient for numerical smoothing of the large density gradients of the moving interface.

In the two-dimensional lock-release problem in a bounded channel, three geometric parameters (in addition to x_0 which is the reference length) appear: the height of the lock, h_0; the height of the ambient fluid, H; and the total length of the channel, x_{w}.

The initial conditions at $t = 0$ are

$$\boldsymbol{v} = \boldsymbol{0} \quad (0 \leqslant x \leqslant x_{\mathrm{w}}, \ 0 \leqslant z \leqslant H) \tag{4.6}$$

and

$$\phi = \begin{cases} 1 & (0 \leqslant r \leqslant 1, \ 0 \leqslant z \leqslant h_0) \\ S(1 - z/H) & \text{elsewhere.} \end{cases} \tag{4.7}$$

The boundary conditions for $t \geqslant 0$ are

$$\boldsymbol{v} = \boldsymbol{0} \ \text{(on the bottom and sidewalls)}; \tag{4.8}$$

$$w = 0, \quad \text{and no shear} \quad (z = H); \tag{4.9}$$

and

$$\hat{n} \cdot \nabla \phi = 0 \quad \text{(on all boundaries).} \tag{4.10}$$

These conditions contain some simplifications, in particular (4.9), which is the frictionless 'rigid lid' approximation for the free surface. In practical situations the free upper surface may have a height perturbation of magnitude ϵ during the flow. In addition, we assume that the lock is removed instantaneously and without any perturbation to the fluid, and that the flow is laminar.

We note in passing that the SW model can be regarded as a solution of the foregoing equations with $\epsilon = Re^{-1} = \mathscr{D} = 0$, under the assumptions that $\boldsymbol{v} = \boldsymbol{0}$ and ϕ retains its initial value outside the domain $0 \leqslant x \leqslant x_N, 0 \leqslant z \leqslant h(r,t)$, while inside this domain $\phi = 1$, $u = u(x,t)$, and the left-hand side of the vertical momentum equation is negligibly small. The scaling here is, for numerical convenience, slightly different from the more insightful one which was used for the SW formulation, but the results are presented with the scaling (2.9) and (2.10).

The foregoing system of equations and boundary conditions was solved by a time-marching, finite-difference discretization method. The details are described by Hallworth *et al.* (2001) and will not be repeated here. The addition of stratification did not create any special numerical difficulties.

Briefly, the method is based on forward-time discretization of the velocity compo-

nents, with implicit pressure terms. For each time step the continuity equation for the 'new' velocity field yields an elliptic equation for the 'new' pressure field.

The spatial discretization is performed on a staggered grid with il radial intervals and jl stretched axial intervals. The variables P and ϕ are defined at mid-cell positions denoted (i, j), u is defined at positions $(i \pm \frac{1}{2}, j)$ and w is defined at $(i, j \pm \frac{1}{2})$. Central spatial differences were used, with the exception of forward and backward differences for the advection terms in the density transport equation (4.4), which was treated by a MacCormack method to avoid spurious oscillations associated with the discontinuity of ϕ at the interface between the current and the ambient. For this purpose we also used artificial diffusion, i.e. a larger value of $\mathcal{D}$ than dictated by molecular diffusion. This is justified by the fact that in the physical salt-water system used in the laboratory experiments, the value of the Schmidt number $\sigma = 700$, and hence the resulting diffusion layer during the time of propagation of the current considered here is very thin, beyond the resolution of feasible numerical grids. The truncation errors are second order in both time and space, and the space and time steps were chosen with the aim of achieving accuracies of about 1% in the velocity and ϕ fields. Two different grids and various time steps were used to verify convergence. The major computational effort was invested in the solution of the discretized Poisson equation for $P_{i,j}$ at all grid points for each time step, by a bi-conjugate gradient method.

The simulations discussed here were obtained for a channel of length $x_w = 4$, the typical grid had 160 horizontal and 200 stretched vertical intervals, and the typical time step was 2×10^{-3}. Hereafter we use again the scaling given by (2.9) and (2.10).

First, for the verification of the numerical code, results pertinent to the configuration of experiments 6 and 19 of MLSM were computed ($H = 3, h_0/x_0 = 0.25$ in both cases, and $S = 0.42$ and 0.71, $\epsilon = 0.071$ and 0.080, respectively). In the computations we used the value $Re = 7.7 \times 10^4$ (defined as $g'^{1/2}x_0^{3/2}/v$) which is compatible with the experiments. The velocity of propagation predicted by the present numerical results was close to constant, and using it we calculated the values of χ, see (3.1), as 0.43 for experiment 6 and 0.26 for experiment 19. The experimental values reported by MLSM (in appendix A, column Fr) are 0.44 and 0.26, which we consider in excellent agreement with the present computations. (We rounded the results to two digits to reflect the expected accuracy in both experiments and computations.)

Next, we performed runs for a configuration with $H = 5$, $h_0/x_0 = 0.333$, $\epsilon = 0.07$ and various values of S. We used the computational value $Re = 10^5$. We recall that MLSM considered only $H \leqslant 3$ and values of h_0/x_0 different from 0.333.

Results for currents with $S = 0.5$ and 0.8 are displayed in figure 7. In both cases the propagation in the computed range is at constant velocity, in accordance with the SW theory prediction. The computed values of the speed of propagation for $S = 0, 0.5$ and 0.8 are $0.61, 0.46$ and 0.32, respectively, and the SW approximation for these cases predicts the velocity $u_N = 0.73, 0.53$ and 0.37. The SW results are about 15% larger than the numerical results, but the effect of stratification is accurately captured: the increase of stratification from $S = 0$ to 0.5 and 0.8 causes a decrease of u_N of about 25% and 48% in the numerical results, almost exactly as predicted by the SW theory. (We note again that discrepancies of this order of magnitude between numerical and SW results are acceptable on account of the approximate background of the latter approach, see also Klemp *et al.* 1994, §4. It appears that the SW approximation with the nose condition (2.23) provides less accurate u_N for large values of H, which can be attributed to more prominent viscosity and mixing effects. This topic, however, requires a separate investigation.)
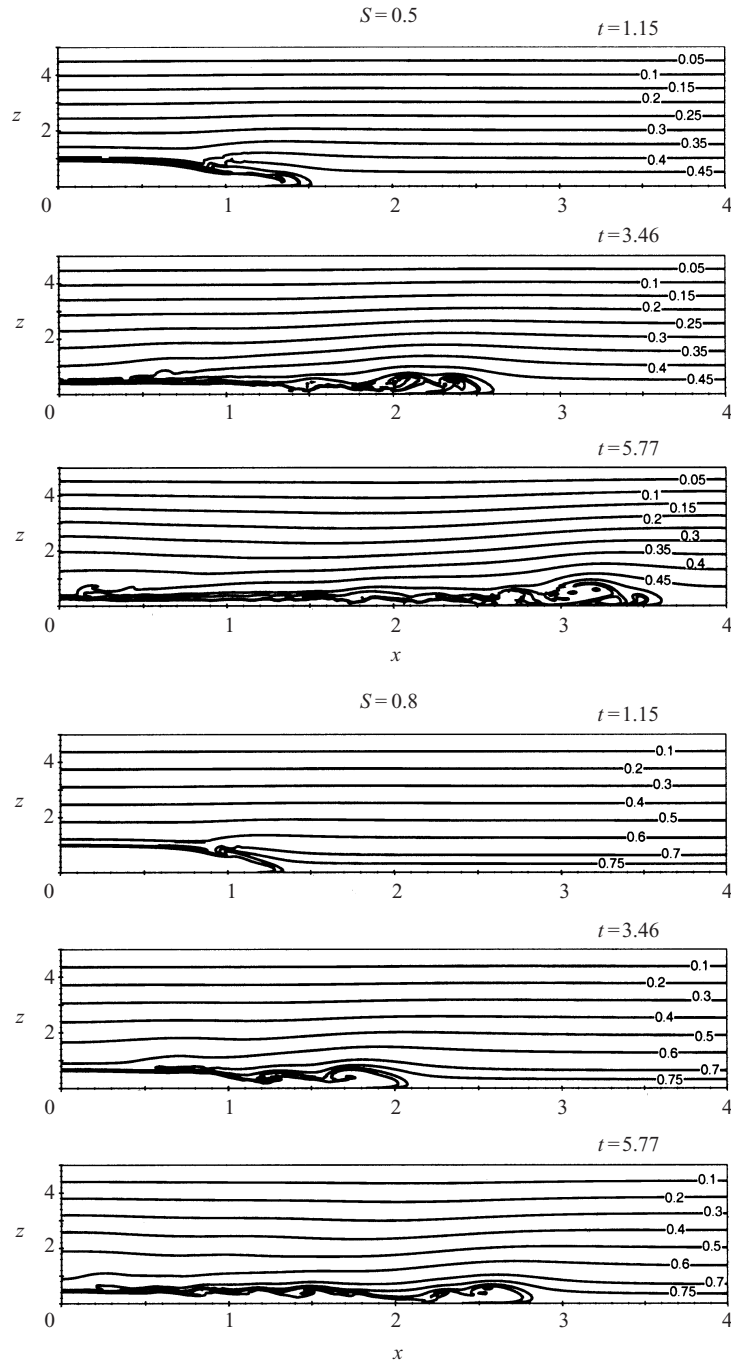
FIGURE 7. Numerical results: contour lines of the density function ϕ at various times, for $S = 0.5$ and 0.8. (Recall that initially, in the dense fluid $\phi = 1$, while in the ambient $\phi = 0$ at the top and $\phi = S$ at the bottom.)

5. Concluding remarks

The shallow-water analysis presented here seems to capture well the effects of stratification on the propagation of the gravity current, at least for the initial 'slumping' phase. The present shallow-water results for the velocity of propagation of the nose are in good agreement with the experimental results of MLSM in both the parameter dependences and the quantitative values. The finite-difference Navier–Stokes results developed here provide additional reliable support for our investigation. The numerical results, for parameters outside the range covered by MLSM, are also in fair agreement with the shallow-water results.

The analysis proves that, essentially, the stratification reduces the speed of propagation compared with motion in a homogeneous ambient with the same density at $z = H$. Roughly, the effective pressure head that drives the nose of the current is proportional to the density difference at the middle height of the nose, but the Froude number correlation between the velocity and the pressure head is not affected by the stratification. The dependences on the stratification are nonlinear and there is, apparently, no simple way to scale out this influence from the governing equations. Nevertheless, we are able to suggest an 'effective' Froude number which is the ratio of the speed of propagation to a reference velocity based on h_0 and a simple estimate of the 'effective' reduced gravity, see (2.28)–(2.29). This ratio varies in a quite narrow range for all the configurations of interest, and therefore is, in our opinion, a good representative synthesis of the process. Practically, the value of this 'effective' Froude number is approximated well by the correlation of Fr as a function of h_N/H in a homogeneous ambient case.

The SW analysis provides a straightforward method for obtaining u_N in the slumping phase in a rectangular geometry, via the solution of a simple nonlinear equation (2.25). For the case of a deep current in an ambient whose density at the bottom is equal to that of the current ($H > 7.4, S = 1$) we obtained the result $u_N = 0.457/H^{1/2}$. This is to be compared with $u_N = 0.746$, which is predicted for the homogeneous ambient ($S = 0$) counterpart.

The incorporation of the stratification in the SW equations (in both rectangular and axisymmetric geometries) and in the nose Froude condition developed in §2 indicates that existing software for the solution of the SW equations with a homogeneous ambient can be extended to study the situation of a stratified ambient with only moderate additional programming effort. We suggest that similar extensions can be readily performed in 'box-model' solvers; the main change in the formulation is to multiply the classical nose velocity by the slow-down factor given in (2.22). Although this may complicate the subsequent analytical solution, the modification of numerical 'box-model' software is straightforward.

We considered only linear stratification in the ambient, but a more complex situation can be treated in a similar way. The nonlinear terms which are expected to appear in the velocity of the characteristics may, however, introduce new effects and difficulties which have no counterpart in the present study.

That our one-layer model, which neglects the influence of internal wave generation and propagation in the ambient, agrees so well with experimental and numerical data suggests that the energy imparted to the internal waves is considerably less than the potential energy transferred into the gravity current. Evidently, further research is necessary to provide a deeper physical understanding of the interaction between the internal waves of the ambient and the propagation of the current which seems to appear at a later stage of motion, as indicated by the experiments of

MLSM. This may necessitate the use of a two-layer SW model which, although straightforwardly derivable from the present formulation, introduces mathematical and physical complications which require special analysis (Klemp *et al.* 1994; Zemach 2002). On the other hand, there is evidence that in some circumstances the 'long time' behaviour of a gravity current influenced by additional circumstances (such as particle-driving and rotation), after the completion of the slumping stage, can be approximated by a rather sophisticated small perturbation to the self-similar solution, as detailed in Hogg, Ungarish & Huppert (2001); this possibility is also an interesting topic for future study.

Appendix. The functions I and χ

A.1. *The function* $I(h_N)$

From the definitions (2.19), (2.24) and (2.25) we obtain

$$I(h_N) = \int_{h_N}^1 \left[\frac{1 - S + S(h/H)}{h} \right]^{1/2} dh. \tag{A 1}$$

Consider first $0 < S < 1$ and write

$$I(h_N) = (1 - S)^{1/2} \int_{h_N}^1 \sqrt{\frac{1 + c^2 h}{h}}\, dh, \tag{A 2}$$

where

$$c = \sqrt{\frac{S}{(1 - S)H}}. \tag{A 3}$$

Letting

$$\eta(h) = \sqrt{\frac{1 + c^2 h}{h}},$$

we can easily verify that

$$\int \sqrt{\frac{1 + c^2 h}{h}}\, dh = -\frac{\eta}{(c^2 - \eta^2)} + \frac{1}{c} \mathrm{arctanh}(\eta/c) \equiv f(\eta).$$

With $\eta_1 = \eta(1)$, $\eta_N = \eta(h_N)$, we obtain

$$I(h_N) = (1 - S)^{1/2} [f(\eta_1) - f(\eta_N)]. \tag{A 4}$$

An approximation for small c^2 can be obtained by using a Taylor expansion of $(1 + c^2 h)^{1/2}$ in the right-hand side of (A 2). The integration of the leading terms gives

$$I(h_N) \approx 2(1 - S)^{1/2} \left[1 + \tfrac{1}{6}c^2 - h_N^{1/2}(1 + \tfrac{1}{6}c^2 h_N) \right]. \tag{A 5}$$

The approximate values are larger than the exact ones, but the relative error is bounded by $c^4/8$. Thus, for $c < 1$ this approximation provides some quick insight into the influence of the stratification on the value of $I(h_N)$.

Consider next the straightforward evaluation of (A 1) for the limiting values of S.
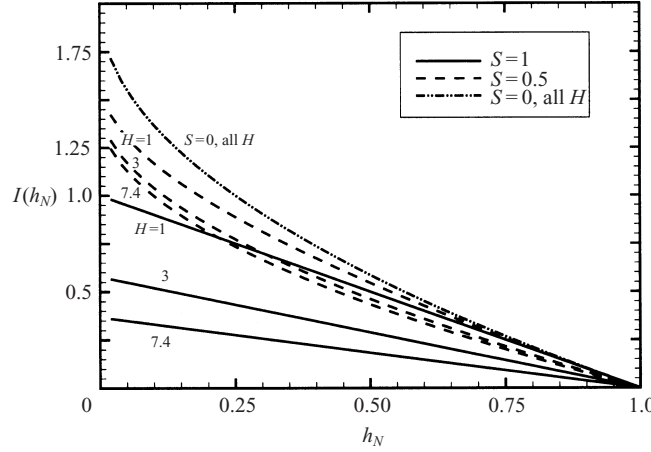
FIGURE 8. I as a function of h_N for various S and H.

For $S = 0$ (homogeneous ambient) we obtain

$$I(h_N) = \int_{h_N}^1 \sqrt{\frac{1}{h}}\,\mathrm{d}h = 2(1 - h_N^{1/2}). \qquad (A\,6)$$

For $S = 1$ (maximal stratified ambient) we obtain

$$I(h_N) = H^{-1/2} \int_{h_N}^1 \mathrm{d}h = H^{-1/2}(1 - h_N). \qquad (A\,7)$$

The typical behaviour of $I(h_N)$ $(0 < h_N < 1)$ is displayed in figure 8. For fixed S and H, I increases monotonically from zero as h_N decreases from 1. For a fixed h_N it decreases with both S and H, i.e. it is bounded by (A 7) and (A 6).

A.2. *The experimental fit*

MLSM showed that their experimental data, reduced according to the left-hand side of (3.1), are accurately described by the empirical fit

$$\chi(S, H) = a(H) - c(H) \log S, \qquad (A\,8)$$

where the coefficients for the values $H = \{1, 1.5, 2, 3\}$ are given by

$$a = \{0.266, 0.229, 0.205, 0.147\}, \quad \text{and} \quad c = \{0.912, 0.916, 0.846, 0.774\}.$$

REFERENCES

BENJAMIN, T. 1968 Gravity currents and related phenomena. *J. Fluid Mech.* **31**, 209–248.

BONNECAZE, R. T., HALLWORTH, M. A., HUPPERT, H. E. & LISTER, J. R. 1995 Axisymmetric particle-driven gravity currents. *J. Fluid Mech.* **294**, 93–121.

BONNECAZE, R. T., HUPPERT, H. E. & LISTER, J. R. 1993 Particle-driven gravity currents. *J. Fluid Mech.* **250**, 339–369.

HALLWORTH, M. A., HUPPERT, H. E. & UNGARISH, M. 2001 Axisymmetric gravity currents in a rotating system: experimental and numerical investigations. *J. Fluid Mech.* **447**, 1–29.

HÄRTEL, C., MEIBURG, E. & NECKER, F. 2000 Analysis and direct numerical simulation of the flow at a gravity current head. Part 1. Flow topology and front speed. *J. Fluid Mech.* **418**, 189–212.

HOGG, A., UNGARISH, M. & HUPPERT, H. E. 2000 Particle-driven gravity currents: asymptotic and box-model solutions. *Eur. J. Mech.* B/*Fluids* **19**, 139–165.

Hogg, A. J., Hallworth, M. A. & Huppert, H. E. 1999 Reversing buoyancy of particle-driven gravity currents. *Phys. Fluids* **11**, 2891–2900.

Hogg, A. J., Ungarish, M. & Huppert, H. E. 2001 Axisymmetric gravity currents: asymptotic analysis of the effects of particle sedimentation and rotation. *Phys. Fluids* **13**, 3687–3698.

Huppert, H. E. 1998 Quantitative modelling of granular suspension flow. *Phil. Trans. R. Soc. Lond.* A **356**, 2471–2496.

Huppert, H. E. 2000 Geological fluid mechanics. In *Perspectives in Fluid Dynamics: A Collective Introduction to Current Research* (ed. G. K. Batchelor, H. K. Moffatt & M. G. Worster), pp. 447–506. Cambridge University Press.

Huppert, H. E. & Simpson, J. E. 1980 The slumping of gravity currents. *J. Fluid Mech.* **99**, 785–799.

Klemp, J. B., Rotunno, R. & Skamarock, W. C. 1994 On the dynamics of gravity currents in a channel. *J. Fluid Mech.* **269**, 169–198.

Maxworthy, T., Leilich, J., Simpson, J. E. & Meiburg, E. H. 2002 The propagation of a gravity current in a linearly stratified fluid. *J. Fluid Mech.* **453**, 371–394 (referred to herein as MLSM).

Rottman, J. & Simpson, J. E. 1983 Gravity currents produced by instantaneous release of a heavy fluid in a rectangular channel. *J. Fluid Mech.* **135**, 95–110.

Simpson, J. E. 1997 *Gravity Currents in the Environment and the Laboratory*. Cambridge University Press.

Ungarish, M. & Huppert, H. E. 1999 Simple models of Coriolis-influenced axisymmetric particle-driven gravity currents. *Intl J. Multiphase Flow* **25**, 715–737.

Zemach, T. 2002 Gravity currents: two-layer and asymptotic extensions. Master's thesis, Technion, Haifa, Israel.